ChemComm

COMMUNICATION

View Article Online
View Journal | View Issue

Cite this: *Chem. Commun.*, 2020, **56**, 6110

Received 12th December 2019,
Accepted 2nd April 2020

DOI: 10.1039/c9cc09671j

rsc.li/chemcomm

Silicon incorporation in polymethine dyes†

Monica Pengshung,[a] Patrick Neal,[b] Timothy L. Atallah,[a] Junho Kwon,[a] Justin R. Caram,*[a] Steven A. Lopez*[b] and Ellen M. Sletten*[a]

Methods to red-shift fluorophores have garnered considerable interest due to the broad utility of low energy light. The incorporation of silicon into xanthene and coumarin scaffolds has resulted in an array of visible and near-infrared fluorophores. Here, we extend this approach to polymethine dyes, another popular fluorophore class, performing experimental and computational analyses. We found that when oxygen was replaced with $SiMe_2$, bathochromic shifts of up to 121 nm and fluorophores with emission above 900 nm were achieved.

Fluorescence is a vital research tool for analysing molecules in complex, dilute environments.[1] Key to the success of fluorescent analyses are fluorophores which have enabled fundamental materials and biological studies; however, due to limitations of light penetration through heterogeneous materials, there has been interest in red-shifting fluorophores to the near-infrared (NIR, 700–1000 nm) region and beyond.[2,3]

In 2008, Xu and coworkers reported that the introduction of silicon into a xanthene chromophore in place of oxygen resulted in a bathochromic shift of 100 nm (Fig. 1A).[4] Following this initial work, the use of silicon to red-shift fluorophores has been applied to oxazine, coumarin, fluorescein and rhodamine dyes (Fig. 1B–D).[5–10] These dyes have been shown to be bright probes with advantageous photostability. We now extend silicon incorporation to another ubiquitous class of fluorophores, polymethine dyes.

Polymethine dyes are known for their narrow absorption bands, high absorption coefficients, and readily tunable λ_{max} within the visible and near-infrared regions. The most common polymethines are cyanine dyes, which have nitrogen-containing heterocycles connected *via* a polymethine chain (Fig. 1E).

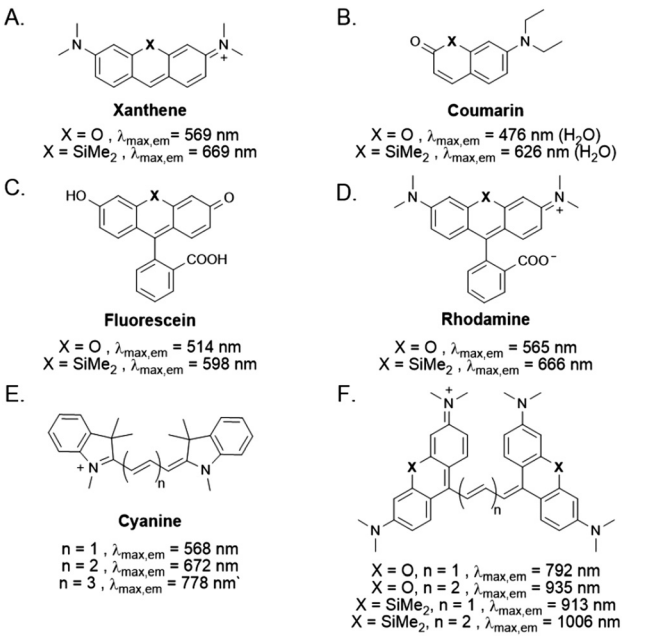

Fig. 1 (A–E) Fluorophore scaffolds. (A) Xanthene.[4] (B) Coumarin.[10] (C) Fluorescein.[9] (D) Rhodamine.[9] (E) Cyanine.[11] (F) This work on silicon polymethines and their oxygen counterparts.[12]

A widely utilized approach to significantly modulate the λ_{max} of cyanine dyes is to vary the length of the polymethine chain, which leads to a ~100 nm red-shift for each additional vinylene unit, though increasing the polymethine chain decreases stability.[11] An alternative strategy to afford large red-shifts is to replace the nitrogen with a different heteroatom such as O, S, Se, and Te.[13] Herein, we demonstrate that the incorporation of silicon into heterocycles for polymethine dyes can impart red-shifts of similar magnitude to extension of the polymethine chain, while also enhancing photostability, resulting in fluorophores with emission above 900 nm (Fig. 1F).

To prepare polymethine fluorophores, heterocycles that can readily react with electrophilic polyene linkers are necessary.

[a] *Department of Chemistry and Biochemistry, University of California, Los Angeles, CA 90095, USA. E-mail: jcaram@chem.ucla.edu, sletten@chem.ucla.edu*
[b] *Department of Chemistry and Chemical Biology, Northeastern University, 360 Huntington Avenue, Boston, Massachusetts 02115, USA. E-mail: s.lopez@northeastern.edu*

† Electronic supplementary information (ESI) available: Supplementary figures and experimental procedures. See DOI: 10.1039/c9cc09671j

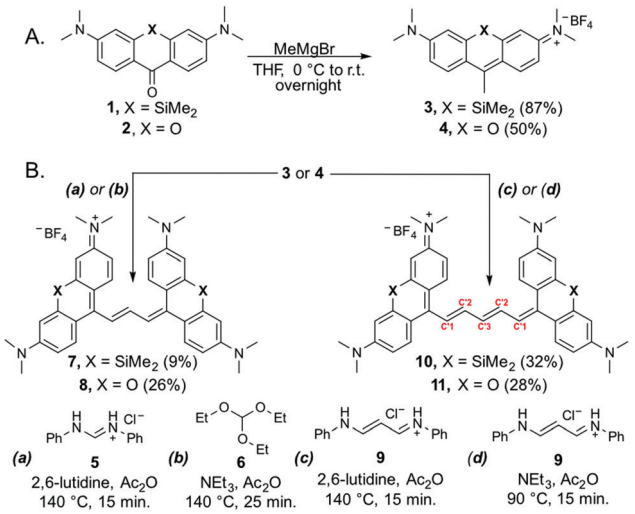

Scheme 1 Synthesis of silicon and oxygen fluorophores studied herein. (A) Heterocycle synthesis. (B) Polymethine dye synthesis. For **7**, conditions (a). For **8**, conditions (b). For **10**, conditions (c). For **11**, conditions (d).

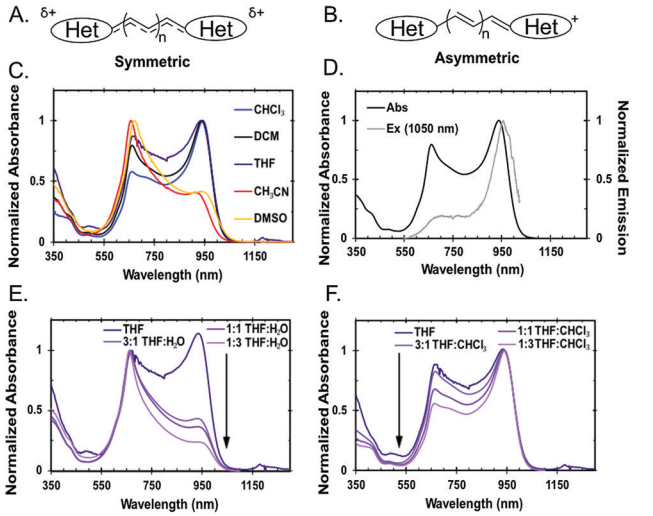

Fig. 3 (A/B) Schematic of symmetric state (delocalized charge, (A)) and asymmetric state (dipolar, charge is localized on one heterocycle, (B)). (C) Absorbance of **10** (normalized to λ_{max}) in a range of nonpolar and polar solvents. (D) Normalized absorption spectra (Abs, black) and excitation spectra (Ex, grey, excitation from 515–1025 nm and collection at 1050 nm) of **10** in DCM. (E) Absorption spectra of **10** normalized at 663 nm in a solution of tetrahydrofuran (THF, 0.01 mM) supplemented with increasing amounts of H_2O. (F) Absorption spectra of **10** normalized at 938 nm in a solution of THF (0.01 mM) supplemented with increasing amounts of $CHCl_3$.

We synthesized xanthone **1** according to literature procedures[14] and treated it with MeMgBr (Scheme 1A) to obtain **3**. Silicon xanthylium **3** proved to be a bright new fluorophore with $\lambda_{max,abs}$ = 646 nm and $\lambda_{max,ems}$ = 673 nm (Fig. 2A, blue). Notably, this is 100 nm red-shifted from the oxygen congener **4**, which we synthesized as a control (Scheme 1A).

To synthesize the first generation of silicon polymethines, **3** was deprotonated with 2,6-lutidine and combined with diphenylformamidinine (**5**) in acetic anhydride (Scheme 1B) to afford **7** as a dark blue solid. Trimethine **7** displayed an absorption band with $\lambda_{max,abs}$ at 854 nm and $\lambda_{max,ems}$ at 913 nm (Fig. 2A and Fig. S1A, red, ESI†). We prepared pentamethine dye **10** through a similar procedure with malonaldehyde bis(phenylimine) HCl (**9**) to yield **10** (Scheme 1B). Pentamethine **10** had a $\lambda_{max,abs}$ at 938 nm and $\lambda_{max,ems}$ at 1006 nm (Fig. 2A and Fig. S1B, black, ESI†).

Silicon polymethines **7** and **10** displayed a large absorption range (550–1000 nm) and contained two distinct peaks at 663 nm, and either 854 nm or 938 nm for **7** and **10**, respectively (Fig. 2A). These spectra are uncharacteristic of traditional cyanine dyes, which have narrow absorbance due to complete electron delocalization (Fig. 3A).[15] Broad absorption spectra has been observed in long chain cyanine dyes (>7 carbon units) due to ground state desymmetrization in which electron delocalization is compromised and dipolar character is observed (Fig. 3B).[15,16] Shorter chain polymethine dyes containing xanthene heterocycles have also been reported to display ground state destabilization, resulting in bimodal absorbance spectra.[17]

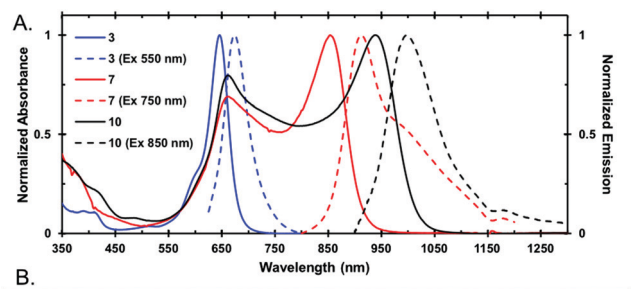

B.

Compound	$\lambda_{max,abs}$ (nm)	$\lambda_{max,ems}$ (nm)	ε (10^4, M^{-1} cm^{-1})	Φ_f (%)	τ (ps)[a]	k_r (ns)[a]	k_{nr} (ns)[a]
3	646	673	3.5 ± 0.4	61 ± 5	-	-	-
7	854	913	3.9 ± 0.4	0.26 ± 0.02	48	0.05	21
10	938	1006	5.9 ± 0.2	0.19 ± 0.01	43	0.03	18

Fig. 2 Photophysical data of silicon fluorophores. (A) Normalized absorbance (solid) and emission (dotted) in dichloromethane (DCM). (B) Photophysical characterization of **3**, **7**, **10** in DCM. [a] Error in Fig. S8 (ESI†).

The absorbance spectra of pentamethine **10** in dichloromethane (DCM) displays a peak ratio of 1 : 1.5 for absorbance at 663 nm and 938 nm. The peak ratio is concentration independent (Fig. S2, ESI†), leading us to ascribe the bimodal absorbance to the presence of asymmetric and symmetric states. We performed a solvatochromism study on **10** (Fig. 3A), which revealed that polar solvents such as dimethyl sulfoxide and acetonitrile resulted in the 633 nm peak dominating by 2.5 fold (Fig. 3C). More systematically studying the effect of polar solvents through the addition of water or chloroform to **10** in THF indicate the 633 nm peak is favoured as solvent polarity is increased (Fig. 3E and F). Mixtures of THF and phosphate buffered saline show similar dominance of the 633 nm peak (Fig. S3, ESI†). Collectively, these results are consistent with previous findings that polar environments are able to stabilize the asymmetric state.[18] Solvactochromism studies of **7** are comparable to **10** (Fig. S4, ESI†). Interestingly, the $\lambda_{max,abs}$ of the asymmetric state of trimethine **7** is similar to pentamethine **10**, while their symmetric states differ by 84 nm. We attribute this to the asymmetric state having significant heterocycle character, with the heterocycle being a good chromophore itself.

To further explore the hypothesis of ground state desymmetrization, we employed quantum mechanical calculations. We first performed a conformational search to identify the global and local minima of **10**. These structures were then optimized with the hybrid density functional M06-2X[19] with the 6-31+G(d,p) basis set in the gas phase and implicit solvent H_2O using Gaussian 16.[20] No gas phase geometries exhibited structural asymmetries nor did the lowest energy conformer in H_2O (**10-H_2O-A**); however, two accessible solvated conformers **10-H_2O-B** and **10-H_2O-C** at 0.6 and 1.5 kcal mol^{-1} higher in free energy, respectively, were found to display asymmetry (Fig. S5, ESI†). Computationally, bond length alternation (BLA) and charge alternation (CA) are characteristic metrics for assessing ground state desymmetrization.[17] Analysis found that **10-H_2O-B** displayed BLA and CA (Fig. S6A and B, ESI†). However, the desymmetrization was small in magnitude, with only 0.17*e* (elementary charge) transferred to one heterocycle (Fig. 4A).

Therefore, we considered the role of dynamic structures resulting from accessible vibrational modes to simulate absorbance spectra (Fig. S7, ESI†). Vertical excitations, calculated with configuration interaction of singles with a correction to doubles method [CIS(D)][21,22] with the cc-pVDZ basis set and resolution of the identity (RI) technique in ORCA 4.0.1[23,24] were computed on 50 Wigner sampled structures from the lowest energy *anti* and *syn* conformers of **10**.‡ Structures with the most red-shifted λ_{max} show complete electron delocalization of the highest occupied molecular orbital (HOMO) and lowest occupied molecular orbital (LUMO) (Fig. 4B), whereas sampled geometries shifted to the 550–700 nm region show a desymmetrized HOMO and LUMO (Fig. 4C). In the desymmetrized structures, the electron density is localized on the heterocycle, consistent with the experimentally observed peak at 663 nm.

While the absorption of the silicon-containing polymethine dyes was broad and bimodal, the emission was well-defined. The quantum yields were low (Φ_F < 0.30%) and excited state lifetimes ranged from 43–48 ps (Fig. 2B and Fig. S8, ESI†).[25] The narrow emission band is attributed to emission solely from the symmetrical state, which was confirmed with the excitation spectra for both **7** and **10** (Fig. 3D, grey and Fig. S4, ESI†).[26]

To showcase the direct benefit of silicon incorporation into the polymethine scaffold, we prepared oxygen congeners **8** and **11** (Scheme 1B and Fig. S9, ESI†) which were hypsochromically shifted (Fig. 5A and B). The red-shift between silicon fluorophores and oxygen is normally attributed to a lowered LUMO energy, caused by σ*–π* conjugation.[27] However, our calculations suggest that the LUMO of **11** is higher in energy than **10** because of a destabilizing out-of-phase interaction between the oxygen lone pair and the π orbitals in **11** (Fig. S10, ESI†).

We found that the degree of red shift between the O and Si containing fluorophores decreased as the polymethine linker increased. The absorbance difference at λ_{max} for the trimethines was 79 nm (1194 cm^{-1}) while the pentamethines was only 42 nm (500 cm^{-1}) (Fig. 5A). The difference in emission is larger for the trimethines than the pentamethines ($\Delta\lambda_{max}$ = 121 and 71 nm, respectively, Fig. 5B). The smaller shifts in absorbance are likely due to contributions from the asymmetric state. Overall, the incorporation of silicon into polymethine fluorophores in place of oxygen results in bathochromic shifts of the symmetric state by 70–100 nm, on par with extension of the polymethine chain and consistent with incorporation of silicon into other fluorophore scaffolds.[8,9]

Finally, another advantage commonly cited for the use of silicon fluorophores is increased photostability.[5,8] We evaluated

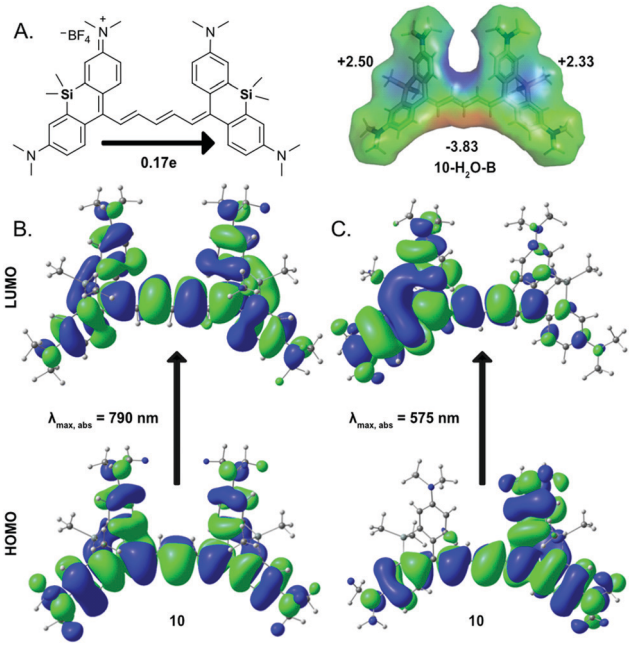

Fig. 4 (A) Conformer **10-H_2O-B** shows desymmetrization of 0.17*e* charge transfer toward the right heterocycle represented schematically and by electron density map. (B/C) Frontier molecular orbitals of Wigner sampled structures of **10** computed with CIS(D)/cc-pVDZ-RI correspond to (B) $\lambda_{max,abs}$ of 790 nm, show complete electron delocalization or (C) $\lambda_{max,abs}$ of 575 nm, show asymmetric character.

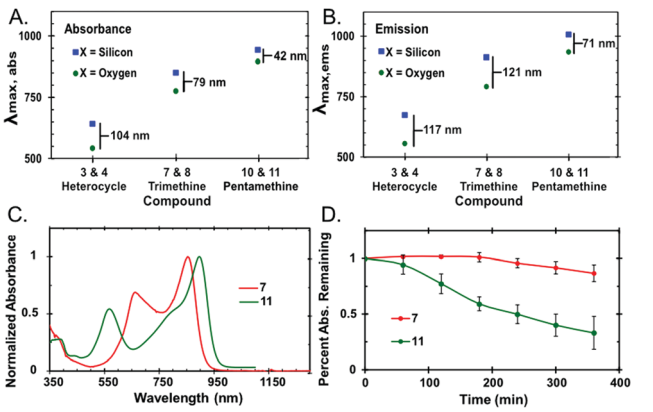

Fig. 5 Comparison of silicon and oxygen xanthene polymethines. (A and B) λ_{max} of silicon- (blue square) and oxygen- (green circle) containing polymethine fluorophores in DCM. The values depicted on the plot indicate the degree of red-shift imparted by silicon. (A) Absorbance. (B) Emission. (C) Normalized absorbance spectra of **7** and **11** in DCM. (D) Percent absorbance remaining at $\lambda_{max,abs}$ of **7** and **11** with continuous irradiation at 730 nm (146 mW cm^{-2}) over 6 hours. Error is the standard deviation of three experiments.

the photostability of silicon *vs.* oxygen fluorophores, focusing on the pair that has the most similar absorption: trimethine **7** and pentamethine **11** (Fig. 5C). We found that **11** began photobleaching rapidly, while **7** was unchanged over three hours (Fig. 5D). Upon calculation of the photobleaching rate constants, we quantified silicon-containing polymethine **7** to be six-fold more stable than **11** (Fig. S11, ESI†). Photobleaching of pentamethine **10** under the same conditions showed a similar decrease as **7**, suggestive that silicon incorporation plays an important role in increasing the photostability. In comparison to other commercial fluorophores, **7** was more stable than HITCI (1,1′,3,3,3′,3′-hexamethylindotricarbocyanine iodide) but less stable than rhodamine B (Fig. S11, ESI†).

We further explored the pathways of degradation for these dyes. Photobleaching of cyanines are generally caused by $^1O_2$ mediated photolysis of the polymethine chain.[27] Thus, **10** and **11** were subjected to $^1O_2$ and analysed for photodegradation products *via* liquid chromatography mass spectrometry (LCMS, Fig. S12, ESI†). We found that **11** degraded quickly (<1 hour) and cleaved at C-1′ of the polymethine chain as anticipated.[28] Surprisingly, **10** reacted slowly, only showing complete degradation at 17 hours. Unlike its oxygen counterpart, **10** degraded into a multitude of products suggesting that silicon incorporation deactivated the $^1O_2$ reactivity at C-1′. We compared this photostability to acid and base stability of **7**, **8**, **10**, and **11** where we found that the oxygen congeners (**8**, **11**) were more stable to base and similarly stable to acid as compared to **7** and **10** (Fig. S13–S16, ESI†).

In summary, we have demonstrated that incorporation of silicon into polymethine dyes is a valid approach to red shift this class of fluorophores and is on par with vinylene chain extension. We prepared tri- and pentamethines with xanthene-derived heterocycles which were 70–100 nm red-shifted and six to ten-fold more photostable compared to oxygen analogues. The xanthene-derived heterocycles, while providing an efficient avenue for the synthesis of silicon polymethine dyes, also promoted ground state desymmetrization, which resulted in a broad, bimodal absorption spectrum and a decreased presence of the emissive species. Looking forward, the implementation of silicon into polymethine heterocycles that do not promote desymmetrization should provide avenues for the creation of deeply red-shifted (>900 nm) fluorophores with high photostability.

We acknowledge research funding from Sloan Research Award (FG-2018-10855 to E. M. S.), NIH (1R01EB027172-01 to E. M. S.), NSF (1940307 to S. A. L.), DOE BES (DE-SC0019245 to J. R. C.), Ms C. Shapazian (to P. N.) and instrumentation funding through the NSF MRI (CHE-1048804), NIH (1S10OD016387-01) and computing resources provided by the Massachusetts Green High-Performance Computing Center (MGHPCC). We thank I. Lim, Dr J. Li, Dr J. Cox, and the Northeastern Research Computing Team for discussions.

Conflicts of interest

There are no conflicts to declare.

Notes and references

‡ We classified structures with polymethine substituents pointed away from each other as *anti*, while structures with polymethine substituents pointed towards each other as *syn*.

1 L. D. Lavis and R. T. Raines, *ACS Chem. Biol.*, 2008, **3**, 142–155.
2 J. V. Frangioni, *Curr. Opin. Chem. Biol.*, 2003, **7**, 626–634.
3 R. Weissleder, *Nat. Biotechnol.*, 2001, **19**, 316–317.
4 M. Fu, Y. Xiao, X. Qian, D. Zhao and Y. Xu, *Chem. Commun.*, 2008, 1780.
5 J. B. Grimm, T. A. Brown, A. N. Tkachuk and L. D. Lavis, *ACS Cent. Sci.*, 2017, **3**, 975–985.
6 G. Lukinavičius, K. Umezawa, N. Olivier, A. Honigmann, G. Yang, T. Plass, V. Mueller, L. Reymond, I. R. Corrêa Jr, Z.-G. Luo, C. Schultz, E. A. Lemke, P. Heppenstall, C. Eggeling, S. Manley and K. Johnsson, *Nat. Chem.*, 2013, **5**, 132–139.
7 Y. Kushida, T. Nagano and K. Hanaoka, *Analyst*, 2015, **140**, 685–695.
8 A. Choi and S. C. Miller, *Org. Lett.*, 2018, **20**, 4482–4485.
9 T. Ikeno, T. Nagano and K. Hanaoka, *Chem. – Asian J.*, 2017, **12**, 1435–1446.
10 C. Li, T. Wang, N. Li, M. Li, Y. Li, Y. Sun, Y. Tian, J. Zhu, Y. Wu, D. Zhang and X. Cui, *Chem. Commun.*, 2019, **55**, 11802.
11 J. L. Bricks, A. D. Kachkovskii, Y. L. Slominskii, A. O. Gerasov and S. V. Popov, *Dyes Pigm.*, 2015, **121**, 238–255.
12 M. P. Shandura, Y. M. Poronik and Y. P. Kovtun, *Dyes Pigm.*, 2005, **66**, 171–177.
13 M. R. Detty and B. J. Murray, *J. Org. Chem.*, 1982, **47**, 5235–5239.
14 T. Pastierik, P. Šebej, J. Medalová, P. Štacko and P. Klán, *J. Org. Chem.*, 2014, **79**, 3374–3382.
15 L. M. Tolbert and X. Zhao, *J. Am. Chem. Soc.*, 1997, **119**, 3253–3258.
16 L. M. Tolbert, *Acc. Chem. Res.*, 1992, **25**, 561–568.
17 S. V. Vasyluk, O. O. Viniychuk, Y. M. Poronik, Y. P. Kovtun, M. P. Shandura, V. M. Yashchuk and O. D. Kachkovsky, *J. Mol. Struct.*, 2011, **990**, 6–13.
18 H. Hu, O. V. Przhonska, F. Terenziani, A. Painelli, D. Fishman, T. R. Ensley, M. Reichert, S. Webster, J. L. Bricks, A. D. Kachkovski, D. J. Hagan and E. W. Van Stryland, *Phys. Chem. Chem. Phys.*, 2013, **15**, 7666.
19 Y. Zhao and D. G. Truhlar, *Theor. Chem. Acc.*, 2008, **120**, 215–241.
20 M. J. Frisch, G. W. Trucks, H. B. Schlegel, G. E. Scuseria, M. A. Robb, J. R. Cheeseman, G. Scalmani, V. Barone, G. A. Petersson, H. Nakatsuji, X. Li, M. Caricato, A. V. Marenich, J. Bloino, B. G. Janesko, R. Gomperts, B. Mennucci, H. P. Hratchian, J. V. Ortiz, A. F. Izmaylov, J. L. Sonnenberg, D. Williams-Young, F. Ding, F. Lipparini, F. Egidi, J. Goings, B. Peng, A. Petrone, T. Henderson, D. Ranasinghe, V. G. Zakrzewski, J. Gao, N. Rega, G. Zheng, W. Liang, M. Hada, M. Ehara, K. Toyota, R. Fukuda, J. Hasegawa, M. Ishida, T. Nakajima, Y. Honda, O. Kitao, H. Nakai, T. Vreven, K. Throssell, J. A. Montgomery, Jr., J. E. Peralta, F. Ogliaro, M. J. Bearpark, J. J. Heyd, E. N. Brothers, K. N. Kudin, V. N. Staroverov, T. A. Keith, R. Kobayashi, J. Normand, K. Raghavachari, A. P. Rendell, J. C. Burant, S. S. Iyengar, J. Tomasi, M. Cossi, J. M. Millam, M. Klene, C. Adamo, R. Cammi, J. W. Ochterski, R. L. Martin, K. Morokuma, O. Farkas, J. B. Foresman and D. J. Fox, *Gaussian 16, Revision A.03*, 2016.
21 M. Head-Gordon, R. J. Rico, M. Oumi and T. J. Lee, *Chem. Phys. Lett.*, 1994, **219**, 21–29.
22 M. Head-Gordon, D. Maurice and M. Oumi, *Chem. Phys. Lett.*, 1995, **246**, 114–121.
23 F. Neese, *Wiley Interdiscip. Rev.: Comput. Mol. Sci.*, 2018, **8**, 1327.
24 F. Neese, *Wiley Interdiscip. Rev.: Comput. Mol. Sci.*, 2012, **2**, 73–78.
25 E. Thimsen, B. Sadtler and M. Y. Berezin, *Nanophotonics*, 2017, **6**, 1043–1054.
26 F. Terenziani, O. V. Przhonska, S. Webster, L. A. Padilha, Y. L. Slominsky, I. G. Davydenko, A. O. Gerasov, Y. P. Kovtun, M. P. Shandura, A. D. Kachkovski, D. J. Hagan, E. W. Van Stryland and A. Painelli, *J. Phys. Chem. Lett.*, 2010, **1**, 1800–1804.
27 S. Yamaguchi and K. Tamao, *J. Chem. Soc., Dalton Trans.*, 1998, 3693–3702.
28 R. Nani, J. A. Kelley, J. Ivanic and M. J. Schnermann, *Chem. Sci.*, 2015, **6**, 6556–6563.